ChemComm

View Online
Dynamic Article Links

Cite this: *Chem. Commun.*, 2011, **47**, 10797–10799

www.rsc.org/chemcomm

COMMUNICATION

Enhancement of visible light photocatalysis by grafting ZnO nanoplatelets with exposed (0001) facets onto a hierarchical substrate†

Shan He,[a] Shitong Zhang,[a] Jun Lu,[a] Yufei Zhao,[a] Jing Ma,[b] Min Wei,*[a] David G. Evans[a] and Xue Duan[a]

Received 19th July 2011, Accepted 24th August 2011
DOI: 10.1039/c1cc14360c

A ZnO nanocatalyst with a high percentage exposure of (0001) facets embedded on a hierarchical flower-like matrix has been prepared by an *in situ* topotactic transformation of a layered double hydroxide precursor, and exhibits significantly higher visible light photocatalytic performance than other ZnO nanomaterials with fewer exposed (0001) facets.

Recently, the chemistry of semiconductors has attracted intense interest in terms of both fundamental research and for their technological applications in photocatalysis, solar energy conversion, and water splitting.[1–3] Among various semiconductors, zinc oxide (a schematic illustration of the structure of hexagonal wurtzite ZnO is shown in Scheme S1, ESI†) with a direct band gap of 3.37 eV has been widely used as a photocatalyst because of its high quantum efficiency, thermal and chemical stability as well as its nontoxicity.[4,5] Because a photocatalytic reaction occurs at the interface between the catalyst and the reactant, the photocatalytic activity is strongly dependent on the surface morphology and electronic structure.[6] Recently, the important influence of the nature of the exposed surfaces of ZnO crystals on photocatalytic efficiency was reported by Jang *et al.* and McLaren *et al.*, who demonstrated that the terminal polar (0001) facet of ZnO is mainly responsible for its photocatalytic activity.[7,8] It is therefore to be expected that preferential growth leading to a high degree of exposure of the (0001) facets of ZnO is one key to enhancing its catalytic activity. In addition, the aggregation of nanoparticles in a reaction system is a serious problem for nanocatalysts, and leads to low dispersion and suppresses the effective exposure of such highly active facets.[9] Therefore there are two prerequisites for obtaining ZnO nanocatalysts with high efficiency: a high degree of orientation and high dispersion. The fabrication of nanoscale ZnO photocatalysts simultaneously satisfying these two requirements remains a long-standing and fundamental scientific problem.

[a] *State Key Laboratory of Chemical Resource Engineering, Beijing University of Chemical Technology, Beijing 100029, P. R. China. E-mail: weimin@mail.buct.edu.cn; Fax: +86-10-64425385; Tel: +86-10-64412131*
[b] *Mesoscopic Chemistry of MOE, Nanjing University, Nanjing 210093, P. R. China*

† Electronic supplementary information (ESI) available: Experimental and computational details; structure and morphology characterization of F-LDH, F-MMO and comparison samples. See DOI: 10.1039/c1cc14360c.

Layered double hydroxides (LDHs) are a class of two-dimensional (2D) anionic clays consisting of positively charged brucite-like host layers and exchangeable interlayer anions.[10,11] The calcination of LDHs at a moderate temperature leads to a topotactic transformation to mixed metal oxides (MMOs), which have been widely used as catalysts, supports and adsorbents for environmental remediation.[12,13] This topotactic transformation provides an effective approach for the fabrication of metal oxide nanoparticles which are grafted within an amorphous matrix, giving rise to a high dispersion of immobilized nanoparticles since agglomeration is effectively inhibited. Recently, hierarchical semiconductors (*e.g.*, Bi_2O_3, TiO_2, ZnO) with controllable morphology, orientation, and dimensions have been fabricated *via* various chemical and physicochemical methods, and shown to exhibit superior photocatalytic behavior to bulk materials.[14] In our previous work, a method of atomic layered deposition followed by *in situ* growth on a biological substrate was shown to offer a means of fabricating hierarchical MMO materials with high photocatalytic activity.[15]

In this work, we report the preparation of ZnO nanoplatelets with a high degree of exposure of (0001) facets embedded in a hierarchical flower-like matrix using the *in situ* topotactic transformation of an LDH precursor, and show that this leads to an enhancement of photocatalytic performance under visible light irradiation when compared with other ZnO nanocatalysts with fewer exposed (0001) facets.

In a typical procedure, amorphous Al_2O_3 microspheres as both support and Al source were added to a solution of NH_4NO_3 and $Zn(NO_3)_2{\cdot}6H_2O$ and the mixture was hydrothermally treated in an autoclave at 80 °C for 48 h. The resulting product (denoted as F-LDH) was separated by centrifugation and washed thoroughly with water and ethanol. Fig. S1 (ESI†) shows the XRD patterns of the amorphous Al_2O_3 microspheres and the as-synthesized F-LDH. A series of reflections which can be indexed to a pristine ZnAl-LDH phase were observed for F-LDH (Fig. S1b, ESI†). Scanning electron microscope (SEM) images (Fig. S2, ESI†) show that the amorphous Al_2O_3 microspheres have a particle diameter of 2–4 μm, while the as-synthesized F-LDH sample is composed of numerous frizzy nanoflakes (~1 μm in width and ~20 nm in thickness) intercrossing with each other and grafted to the substrate. The sectional image of an F-LDH microsphere

(Fig. S2d, ESI†) confirms that the LDH flower-like shell (~1.5 μm in height) is grafted to the amorphous Al_2O_3 core. The growth of the F-LDH can be explained by a homogeneous nucleation mechanism as described in our previous work.[16] High resolution transmission electron microscopy (HRTEM) also shows the presence of the flower-like LDH shell and the amorphous Al_2O_3 core (Fig. S3a, ESI†). The TEM image of a single nanoflake is shown in Fig. S3b (ESI†) and a hexagonal lattice with spacing 0.30 nm, corresponding to the (100) planes of a ZnAl-LDH phase,[15] was observed in the lattice fringe image (inset in Fig. S3b, ESI†).

The changes in crystal structure and morphology during calcination of the F-LDH precursor were investigated in detail. The XRD reflections of the resulting F-MMO material (Fig. S4, ESI†) can be indexed to a hexagonal wurtzite ZnO phase (JCPDF 36-1451). The mass percentage of the ZnO phase in F-MMO was found to be 34% (wt%) by means of inductively coupled plasma–atomic emission spectroscopy (ICP–AES). Furthermore, the SEM images of the resulting F-MMO (Fig. 1a and b) show that it inherits the original flowerlike morphology of the F-LDH precursor, and no agglomeration or sintering of adjacent nanoflakes was observed. More interestingly, Fig. 1c shows that there is an abundance of well-dispersed nanoplatelets on both sides of the MMO nanoflakes. The high magnification SEM image (Fig. 1d) of a single MMO nanoflake reveals that hexagonal nanoplatelets with diameter of 10–50 nm and thickness of 6–8 nm (inset in Fig. 1d) were immobilized on the nanoflake substrate with high dispersion.

HRTEM was employed to confirm the structure of the hexagonal nanoplatelets on the F-MMO nanoflake. It can be observed from Fig. 2a that hexagonal nanoplatelets are immobilized on the substrate with a high degree of orientation, consistent with the SEM image (Fig. 1d). A single hexagonal nanoplatelet is shown in Fig. 2b, and the clear lattice fringes (Fig. 2c) indicate the single crystalline nature of the nanoplatelet. The interplanar spacing is 0.28 nm, which corresponds to the $(10\bar{1}0)$ plane of a hexagonal ZnO phase. The selected area electron diffraction (SAED) pattern (inset in Fig. 2c) along the

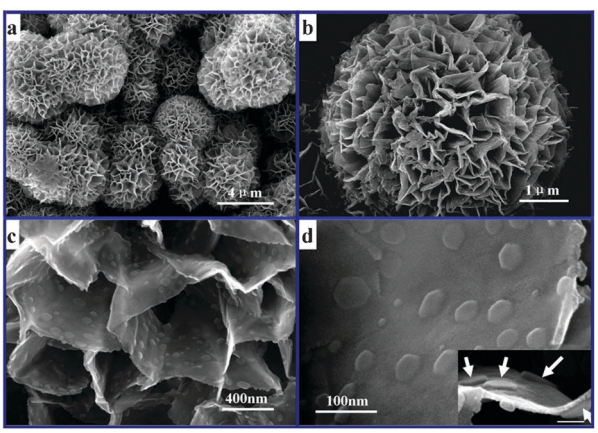

Fig. 1 SEM images of the as-obtained F-MMO sample: (a) an overall view of the F-MMO microspheres; (b) a single F-MMO microsphere; (c) the nanoflakes of a F-MMO microsphere; (d) a portion of a F-MMO nanoflake with hexagonal ZnO nanoplatelets embedded on its surface (inset: the cross section of the F-MMO nanoflake).

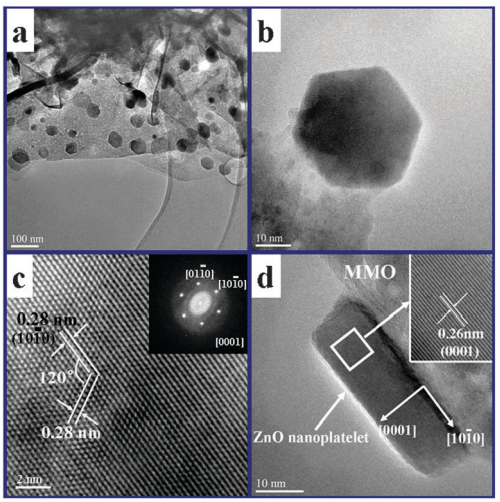

Fig. 2 HRTEM images of the F-MMO sample: (a) a F-MMO nanoflake with ZnO nanoplatelets on its surface; (b) a single-crystalline ZnO nanoplatelet; (c) HRTEM image of (b) (inset: the corresponding SAED pattern of (b) along the [0001] zone axis); (d) the cross section of a ZnO nanoplatelet with exposed (0001) facet embedded on the F-MMO substrate.

[0001] zone axis has regular and clear hexagonal diffraction spots and reveals that the top and bottom surfaces of each ZnO nanoplatelet are the ±(0001) facets, whilst the side surfaces parallel to the *c*-axis can be attributed to the $\{10\bar{1}0\}$ facets of a single crystal. Both the HRTEM and SAED results indicate that the preferred growth direction of ZnO is along $\{10\bar{1}0\}$, which leads to the formation of hexagonal ZnO nanoplatelets with a high degree of exposure of (0001) facets. In contrast, most reported synthetic procedures of wurtzite ZnO nanomaterials result in hexagonal rods elongated along the *c*-axis,[7] since the Zn-terminated (0001) plane has the highest energy among all the facets, and promotes one-dimensional growth along the *c*-axis leading to a preponderance of exposed low energy $\{10\bar{1}0\}$ planes.[8,17]

The reason for the formation of nanoplatelets of ZnO in our case can be understood as follows. During the structural evolution of the F-LDH precursor into the final F-MMO (Scheme S2, ESI†), a topotactic transformation based on the hexagonal structure of LDH is believed to occur, resulting in the formation of hexagonal ZnO nanoplatelets embedded on the F-MMO surface (Fig. S5, ESI†). As a result, hexagonal crystals of ZnAl-LDH nanoflakes serve as both a Zn source and a rigid template, which restrains the fast growth rate of ZnO along the *c*-axis and induces the preferred growth of the nanoplatelets along the $\{10\bar{1}0\}$ direction. This results in the top surface of the ZnO nanoplatelet being terminated by the Zn (0001) facet (as shown in Fig. 2d). The average aspect ratio $(0001/10\bar{1}0)$ observed from Fig. 2d is ~5, corresponding to nearly 50% of the total exposed facets being (0001). The nitrogen adsorption–desorption isotherms and porosity data (see Fig. S6 and detailed discussion in ESI†) show that F-MMO has a rather wide distribution of mesopores (2–25 nm, with a maximum at 4.0 nm) and a specific surface area of 84 $m^2\ g^{-1}$.

The photocatalytic decomposition of Rhodamine B (RhB) under visible light irradiation ($\lambda > 400$ nm) was studied as a probe reaction using the F-MMO sample, with MMO powder

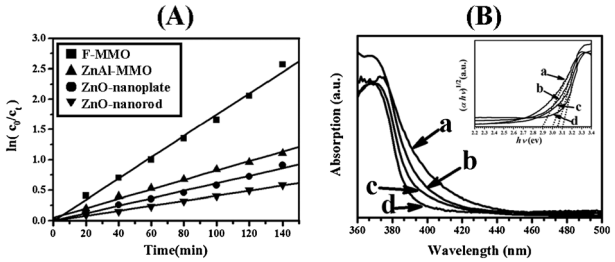

Fig. 3 (A) The pseudo-first order kinetics for the photocatalytic degradation of RhB under visible light irradiation, using F-MMO, MMO, ZnO nanoplates and ZnO nanorods; (B) UV-vis diffuse reflectance spectra of (a) F-MMO, (b) MMO, (c) ZnO nanoplates, (d) ZnO nanorods. Inset: the corresponding plots of $(\alpha h\nu)^{1/2}$ *vs.* $h\nu$ (α = absorption coefficient) used to calculate the band gap energy.

prepared by calcination of a powdered LDH precursor, ZnO nanoplates and ZnO nanorods samples for comparison (see details in ESI†). In control experiments, it was found that both the self-degradation of RhB and photodegradation of RhB by the amorphous Al_2O_3 microspheres under visible light irradiation were negligible (Fig. S7, ESI†). Fig. 3A shows the pseudo-first order kinetics (eqn (1), ESI†) of the degradation of RhB by the four ZnO samples with the pseudo-first order rate constants (k) decreasing in the order: F-MMO > MMO > ZnO nanoplates > ZnO nanorods (see Table S1 in ESI†). The F-MMO showed high photocatalytic efficiency with RhB being fully decomposed after 180 min (Fig. S8, ESI†). The results clearly demonstrate that the F-MMO sample—with its high dispersion and high degree of exposure of (0001) facets—possesses superior visible light photocatalytic activity to ZnO nanorods (with fewer exposed (0001) facets), ZnO nanoplates (with equal exposure of Zn (0001) and O (000$\bar{1}$) facets) and the MMO powder sample (with a high degree of aggregation; Fig. S9, ESI†).

As shown in Fig. 3B, the absorption edge of ZnO-based F-MMO is shifted into the visible light region and shows stronger absorption in the range 400–450 nm compared with the three other ZnO samples. The band gap of the F-MMO is estimated to be ~2.90 eV based on the UV-visible diffuse reflectance spectrum (inset of Fig. 3B), lower than that of the MMO (3.0 eV), ZnO nanoplates (3.04 eV) and ZnO nanorods (3.12 eV). The high visible light photocatalytic behaviour of F-MMO is possibly related to the oxygen defects (*e.g.*, $V_O^{\bullet\bullet}$ and O_i'' defects) present in the exposed (0001) facet. A typical HRTEM image (Fig. S10, ESI†) shows that bending of lattice fringes (Fig. S10a, b1 and 2) and edge dislocation (Fig. S10c and d) were observed, confirming the presence of defects (including oxygen defects) in the (0001) polar surface. It has been reported that a large fraction of polar planes of ZnO favours the formation of more oxygen defects,[18a,b,c] which have a significant impact on the electronic properties, and enhance the efficient separation of electron–hole pairs.[8,18] Therefore, the observed red-shift of the band gap for F-MMO can be explained by the formation of oxygen defects during the *in situ* topotactic transformation of the F-LDH precursor. Furthermore, the ZnO nanoplatelets embedded in the hierarchical F-MMO architecture exhibit a high degree of dispersion and high stability, with the matrix effectively preventing aggregation of nanoparticles and enhancing the efficiency of electron–hole separation. In addition, density functional theory (DFT) calculations were carried out (see details in ESI†) in order to give further insight into the electronic structure. The results show that a lower band gap was obtained for the (0001) surface relative to bulk ZnO and (10$\bar{1}$0) and (000$\bar{1}$) surfaces, accounting for its high visible light photocatalytic activity, in accordance with the experimental results. Furthermore, when the F-MMO catalyst was reused, it maintained a constant photocatalytic activity over 10 consecutive cycles (Fig. S12, ESI†). No obvious changes in its morphology or structure were observed after the reaction (Fig. S13 and S14, ESI†), demonstrating that it can serve as a stable, effective and recyclable photocatalyst.

In summary, a ZnO nanocatalyst with high percentage exposure of (0001) facets grafted on a hierarchical MMO architecture can be prepared by an *in situ* topotactic transformation approach, and the material exhibits excellent photocatalytic performance under visible light irradiation. It is expected that this facile approach can be extended to the preparation of other immobilized metal or metal oxide nanocatalysts with preferential exposure of highly active facets.

This project was supported by the the 973 Program (Grant No.: 2011CBA00504), the National Natural Science Foundation of China, the 111 Project (Grant No.: B07004) and the Collaborative Project from the Beijing Education Committee.

Notes and references

1 M. R. Hoffmann, S. T. Martin, W. Choi and D. W. Bahnemann, *Chem. Rev.*, 1995, **95**, 69.
2 M. Grätzel, *Nature*, 2001, **414**, 338.
3 T. L. Thompson and J. T. Yates Jr, *Chem. Rev.*, 2006, **106**, 4428.
4 Z. L. Wang, *ACS Nano*, 2008, **2**, 1987.
5 S. Sakthivel, B. Neppolian, M. V. Shankar, B. Arabindoo, M. Palanichamy and V. Murugesan, *Sol. Energy Mater. Sol. Cells*, 2003, **77**, 65.
6 (*a*) H. Yang, C. Sun, S. Qiao, J. Zou, G. Liu, S. C. Smith, H. Cheng and G. Lu, *Nature*, 2008, **453**, 638; (*b*) K. Zhou, X. Wang, X. Sun, Q. Peng and Y. D. Li, *J. Catal.*, 2005, **229**, 206.
7 E. S. Jang, J. H. Won, S. J. Hwang and J. H. Choy, *Adv. Mater.*, 2006, **18**, 3309.
8 A. McLaren, T. V. Solis, G. Li and S. C. Tsang, *J. Am. Chem. Soc.*, 2009, **131**, 12540.
9 Z. Liu, D. Sun, P. Guo and J. O. Leckie, *Nano Lett.*, 2007, **7**, 1081.
10 A. I. Khan, L. X. Lei, A. J. Norquist and D. O'Hare, *Chem. Commun.*, 2001, 2342.
11 J. A. Gursky, S. D. Blough, C. Luna, C. Gomez, A. N. Luevano and E. A. Gardner, *J. Am. Chem. Soc.*, 2006, **128**, 8376.
12 (*a*) C. Li, L. Wang, M. Wei, D. G. Evans and X. Duan, *J. Mater. Chem.*, 2008, **18**, 2666; (*b*) M. Zhao, Q. Zhang, W. Zhang, J. Huang, Y. Zhang, D. Su and F. Wei, *J. Am. Chem. Soc.*, 2010, **132**, 14739.
13 H. Liu and E. Z. Min, *Green Chem.*, 2006, **8**, 657.
14 (*a*) L. Zhou, W. Wang, H. Xu, S. Sun and M. Shang, *Chem.–Eur. J.*, 2009, **15**, 1776; (*b*) S. Liu, J. Yu and M. Jaroniec, *J. Am. Chem. Soc.*, 2010, **132**, 11914; (*c*) F. Lu, W. Cai and Y. Zhang, *Adv. Funct. Mater.*, 2008, **18**, 1047.
15 Y. Zhao, M. Wei, J. Lu, Z. L. Wang and X. Duan, *ACS Nano*, 2009, **3**, 4009.
16 H. Chen, F. Zhang, S. Fu and X. Duan, *Adv. Mater.*, 2006, **18**, 3089.
17 J. H. Choy, E. S. Jang, J. H. Won, J. H. Chung, D. J. Jang and Y. W. Kim, *Appl. Phys. Lett.*, 2004, **84**, 287.
18 (*a*) Y. H. Zheng, C. Q. Chen, Y. Y. Zhan, X. Y. Lin, Q. Zheng, K. M. Wei, J. F. Zhu and Y. J. Zhu, *Inorg. Chem.*, 2007, **46**, 6675; (*b*) G. R. Li, T. Hu, G. L. Pan, T. Y. Yan, X. P. Gao and H. Y. Zhu, *J. Phys. Chem. C*, 2008, **112**, 11859; (*c*) V. Ischenko, S. Pozarz, D. Grote, V. Stavarache, K. Fink and M. Driess, *Adv. Funct. Mater.*, 2005, **15**, 1945; (*d*) L. Wang, L. X. Chang, B. Zhao, Z. Y. Yuan, G. S. Shao and W. J. Zheng, *Inorg. Chem.*, 2008, **47**, 1443.